MIT Libraries | DSpace@MIT

MIT Open Access Articles

Origins of the Stokes Shift in PbS Quantum Dots: Impact of Polydispersity, Ligands, and Defects

Massachusetts Institute of Technology

Origins of the Stokes Shift in PbS Quantum Dots: Impact of Polydispersity, Ligands, and Defects

Yun Liu,[†,§] Donghun Kim,[‡,§] Owen P. Morris,[†] David Zhitomirsky,[†] and Jeffrey C. Grossman[*,†]

[†]Department of Materials Science and Engineering, Massachusetts Institute of Technology, Cambridge, Massachusetts 02139, United States

[‡]Computational Science Research Center, Korea Institute of Science and Technology, Seoul 02792, Korea

Ⓢ *Supporting Information*

ABSTRACT: Understanding the origins of the excessive Stokes shift in the lead chalcogenides family of colloidal quantum dots (CQDs) is of great importance at both the fundamental and applied levels; however, our current understanding is far from satisfactory. Here, utilizing a combination of *ab initio* computations and UV−vis and photoluminescence measurements, we investigated the contributions to the Stokes shift from polydispersity, ligands, and defects in PbS CQDs. The key results are as follows: (1) The size and energetic disorder of a polydisperse CQD film increase the Stokes shift by 20 to 50 meV compared to that of an isolated CQD; (2) Franck−Condon (FC) shifts increase as the electronegativities of the ligands increase, but the variations are small (<15 meV). (3) Unlike the aforementioned two minor factors, the presence of certain intrinsic defects such as V_{Cl}^+ (in Cl-passivated CQDs) can cause substantial electron density localization of the band edge states and consequent large FC shifts (100s of meV). This effect arising from defects can explain the excessive Stokes shifts in PbS CQDs and improve our understanding of the optical properties of PbS CQDs.

KEYWORDS: *PbS nanocrystal, colloidal quantum dot, DFT, Stokes shift, defects*
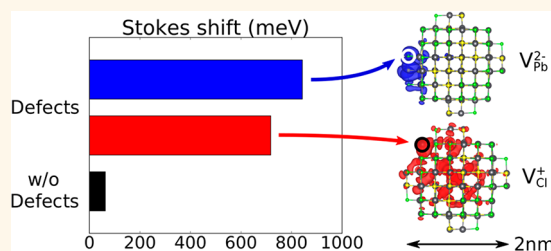
The redshift of an emission spectrum with respect to the corresponding absorption spectrum is known as the Stokes shift. It is an important property in many applications based on semiconductor colloidal quantum dots (CQDs). For example, a large Stokes shift is desired in solar concentrators to minimize photon reabsorption.[1,2] Conversely, in photovoltaics (PVs), the Stokes shift leads to a loss in the open-circuit voltage (V_{oc}), and as a result, it should be minimized to achieve higher power conversion efficiency. PbS is one of the best performing quantum dot-based materials for PV applications, but it suffers from a particularly large Stokes shift that limits its efficiency.[3]

To effectively control the Stokes shift in various CQD-based applications, there must be an improved understanding of its origins. Previous work has identified two different mechanisms responsible for the Stokes shifts: the dark exciton arising from the exciton fine structure and the Franck−Condon (FC) relaxation. In the dark exciton picture, absorption occurs from a valence state that lies deeper than the band edge states to form an exciton, while emission takes place through band edge transitions with the help of phonons, giving rise to red-shifted photons.[4] Another important mechanism of the Stokes shift is the vibrational relaxations upon photoexcitation and is referred to as a FC relaxation. In the presence of an exciton, each atom

of the nanocrystal should experience excited-state forces and undergo consequent structural relaxations, leading to a shift in the total energy of the system.[5,6]

The Stokes shift in II−VI CQDs such as CdSe has garnered particular attentions in the literature, with the focus on excitonic fine structures near the bandedge.[4,7−10] An effective mass model was used to identify the dark exciton in CdSe CQDs.[8−10] In the model, electron−hole exchange interactions and crystal structure anisotropy (wurzite or zinc blende crystal structure of CdSe) split the degenerate 1S band-edge exciton states, wherein the lowest-energy state is optically forbidden (*i.e.*, dark exciton) and the higher energy state is optically allowed (*i.e.*, bright exciton). The Stokes shift in CdSe CQDs is ascribed to the energy splitting between bright and dark exciton states. Another model based on tight-binding approach also supports the argument that the splitting of exciton states is key to explaining the Stokes shift in CdSe CQDs and adds the importance of singlet−triplet splitting for more accurate predictions.[4,5]
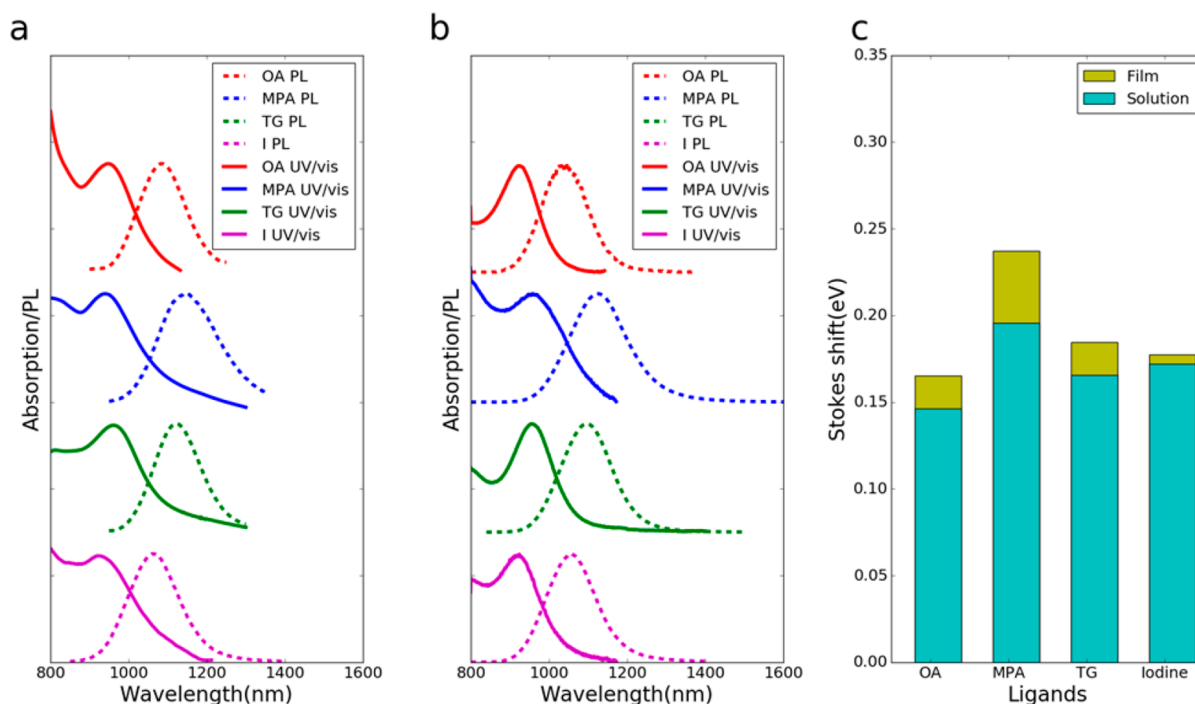
Figure 1. Experimental absorption (solid lines) and emission (dashed lines) of PbS CQDs (a) in films and (b) in dilute solutions. (c) The Stokes shifts of PbS CQDs in films and in solution passivated with oleic acid (OA), mercaptopropionic acid (MPA), 1-thioglycerol (TG), and iodine ligands.

Recently, the Kambhampati group made many efforts to explore the effects of vibronic contributions to the absorption and emission spectra in CdSe CQDs. They demonstrated that CdSe emissions are controlled by strong carrier self-trapping, and its linewidth is strongly modulated by the presence of multiple surface states with varying electron−phonon coupling strength.[11,12] Optical properties such as the Stokes shift are controlled by ligands which delocalizes the excitonic wave function,[11,13,14] and the exciton−phonon coupling strengths are enhanced for smaller CQDs with larger relative surface areas.[11,15] Coherent phonon techniques such as chirp pulse and polarized resolved femtosecond pump/probe were also exploited to successfully measure the exciton−phonon couplings.[16]

Unlike CdSe CQDs, an explanation of the origins of the Stokes shift in the lead chalcogenides (*i.e.*, PbS, PbSe, and PbTe) family of nanocrystals based on the exciton fine structure is challenging.[17,18] Energy splittings between the singlet and triplet states and the manifold quasi-degenerate states near the valence and conduction band edges are only on the order of 20 meV,[19−22] which is too small to explain the 220 meV redshift observed experimentally. Recently, it has been proposed that the presence of midgap state might be responsible for the Stokes shift in PbS CQDs.[23] The role of vibronic contributions in these materials have received comparatively little attention. To the best of our knowledge, FC relaxations in PbS CQDs, as well as the effects of different passivating ligands and intrinsic defects, have not been studied before.

Here, we use both density functional theory (DFT) calculations and UV−vis and photoluminescence (PL) measurements to investigate the origin of the Stokes shift in PbS CQDs, and the contributions of polydispersity, ligands, and defects are quantified. Our results show that the size and energetic disorders in a polydisperse CQD film can increase the

Stokes shifts of 3 nm PbS CQDs by approximately 20 to 50 meV compared to isolated CQDs. Our results are consistent with the recent work which systematically studied the effects of polydispersity on the Stokes shift in PbS CQD.[24] The electronegativity of passivating ligands can also affect the FC shift, but the variation is small and <15 meV. In contrast to these minor factors, our calculations show that intrinsic and stable defects such as V_{Cl}^{+} on the naocrystal surface can cause large FC shifts and may be sufficient to explain the origins of the excessive Stokes shift in PbS CQDs.

RESULTS AND DISCUSSION

Polydispersity. Figure 1a shows the measured absorption and PL spectra of four PbS nanocrystal films capped with different ligands. The absorption band edges are at approximately 950 nm, indicating that the CQDs have a diameter of approximately 3 nm. The PL spectra are significantly redshifted relative to the absorption spectra, signifying a large Stokes shift (165−245 meV) comparable to the values reported previously.[20,23] Figure 1b shows the absorption and PL spectra of the same nanocrystals suspended in dilute solutions. In a typical sample, there is a 5−10% standard deviation in the CQD sizes. Charge carriers can hop from one CQD to neighboring sites with lower band energies before recombination, redshifting the PL spectra. Hopping transport is enhanced in a CQD film, in which the CQDs are closed packed, and hence the electronic couplings are greater than those for CQDs suspended in dilute solutions.[25−27] The redshift due to the size and energetic disorders of a polydisperse CQD film has an additive effect on the intrinsic Stokes shift of individual CQD, and our analysis shows that such effects increase it by approximately 20 to 50 meV (Figure 1c). Our measurements highlight that it is important to distinguish the Stokes shift of CQDs in film and in solution. As CQDs are much sparser in

solution, we can decouple the effects coming from within the CQD itself from ensemble film effects. The impact from sample polydispersity can be minimized by some of the common strategies used to improve the size uniformity of CQDs, such as size selection[28] and stoichiometric control.[29]

It is also worth comparing the sub-band gap reabsorptions between CQDs films and dilute solutions. In a polydisperse CQDs sample, sub-band gap reabsorption occurs when the emitted photons are reabsorbed by larger CQDs or aggregates with a smaller band gap. As we do not observe a defect band in the absorption spectra in our samples, the sub-band gap reabsoption likely arises from the tail end of the distribution. Larger CQDs and aggregates play a much larger role in the film PL spectra, as the charge carriers will eventually migrate to these lower energy centers before emissions.[30] These effects are much less pronounced in dilute solution measurements, where there is a much greater spatial separation between individual CQDs.

We note that a recent work showed film polydispersity arising from nanocrystal aggregation as the dominant factor in the excessive Stokes shift in PbS CQDs.[24] The Stokes shift could be almost eliminated by increasing the ligand concentration, by using nonpolar solvent to prevent CQDs aggregation and extreme dilution of the sample. Our work supports the idea that the energy transfer among CQDs is responsible for a significant amount of excessive Stokes shift; however, our measurements show that the Stokes shifts from isolated CQDs in dilute solutions are still too large (150−195 meV) compared to the values from previous theoretical calculations (<20 meV for similar size CQDs).[21]

Ligands. Surface ligands are essential for maintaining the colloidal stability of CQDs due to their large surface area[31,32] and for modifying their band alignment,[33,34] morphology,[35] and optical properties.[36] In Figure 1, we can observe that different ligands lead to different Stokes shift values. However, no clear trend can be conclusively inferred from the experiments. Previous studies have shown that varying the ligand coverage on CdSe CQDs has minimal impact on the first absorption peak energies.[37] To investigate how ligand chemistry can affect the Stokes shift, we performed a series of DFT calculations that allow us to access parameters that are challenging to obtain experimentally. In particular, we systematically explored the impact of ligand electronegativity on the Stokes shift, focusing on the FC shifts, as the effects of the exciton fine structures in PbS CQDs are known to be negligibly small.

The ideal band gap for PV is approximately 1.3 eV,[38,39] corresponding to a PbS CQD diameter of 3−4 nm. At this diameter, the most commonly observed CQD has the shape of a truncated octahedron[40] terminated by {100} and {111} planes.[41−43] The {111} facets are typically Pb-rich and passivated with ligands, whereas the other facets, such as {100}, do not require any passivation. Following these considerations, we constructed a CQD model with the chemical formula of $Pb_{104}S_{80}X_{48}$, where X is an X-type ligand (an example with X = Cl is shown in Figure 2). The Pb:S ratio is ~1.3:1, and the ratio of Pb ions to ligands is approximately 1:2, thereby satisfying the overall stoichiometry.[44] The diameter and band gap of the DFT-optimized structures are approximately 2.0 nm and 1.2 eV, respectively. Our calculated band gap is smaller than the experimentally observed band gap because of the well-known DFT underestimation of the semiconductor band gap. The orbital contributions to the density of states (DOS) near the Fermi level are very similar to
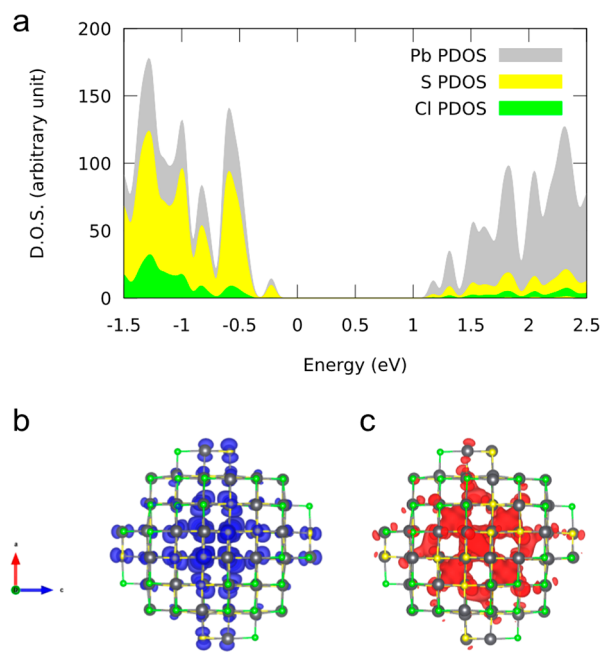

Figure 2. (a) The partial density of states (PDOS) $Pb_{104}S_{80}Cl_{48}$ nanocrystal from Pb, S and Cl species. The band gap is approximately 1.2 eV and trap free. The Fermi level is referenced at 0 eV, and (b) the VBM has predominately S(3p) character, whereas the (c) CBM has mostly Pb(6p) character. The charge densities are delocalized around the core atoms.

other published results, where the valence band and conduction band mainly consist of S(3p) and Pb(6p) orbitals, respectively.[42,44] The charge density distribution shows that the electron wave function of the valence-band maximum (VBM) and conduction-band minimum (CBM) are delocalized over the core atoms, with some contribution along the {100} surface and very little from the {111} surface.

In the field of organometallic chemistry, ligands are classified on the basis of Green's covalent-bond formalism. X-type ligands correspond to 1-electron neutral ligands and include organic ligands such as carboxylic acids (RCOOH), thiols (RSH), and atomic ligands such as halogen atoms.[45] In our calculations, we passivated the {111} surfaces with methanethiol (CH_3SH) and halogen atoms (I, Br, Cl). The ionic radii of ligands decrease from I$^-$ to Cl$^-$, resulting in shorter Pb−X bond lengths. According to the Pauli scale, the effective electronegativity of the surface ligands follows the order of CH_3SH < I < Br < Cl.[46] Ligands with higher electronegativities are also bonded more strongly to the surface Pb atoms, further reducing the average Pb−X bond lengths. Therefore, CQDs capped with more electronegative ligands have a smaller effective size with larger resulting FC shifts (Figure 3a). This phenomenon, that is, the increase in Stokes shifts with decreasing size of the nanocrystal, is well-known.[20,47] The variations in FC shifts between different ligands are observed only around 15 meV, and the effects will be further diminished as the size of the CQDs increases. Although manipulating the ligand electronegativities can change the FC shift, this effect is too small to explain the excessive Stokes shift observed experimentally.

The atomic displacement is defined as the difference between the atomic positions of the same atom when the CQD is in the electronic ground state $\{R_{gs}\}$ and the excited triplet states $\{R_{xs}\}$. From the charge density plots, we observe that the electron densities of the VBM and CBM are delocalized over the interior
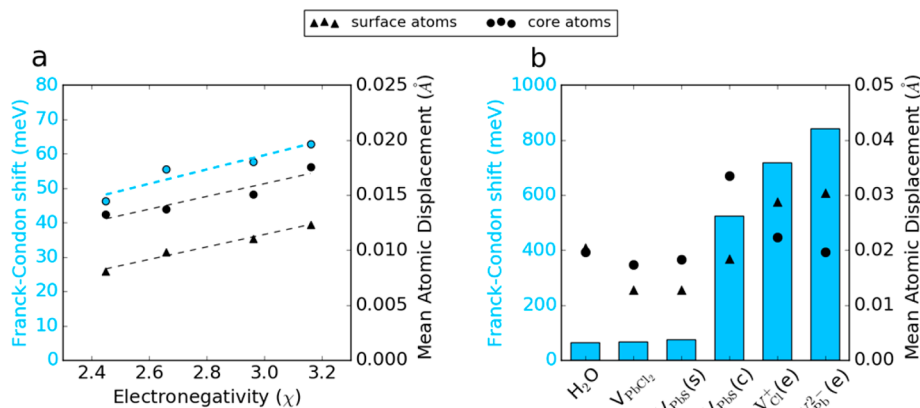
Figure 3. (a) The FC shifts and average atomic displacements between the ground-state $\{R_{gs}\}$ and the excited-state $\{R_{xs}\}$ configurations of $Pb_{104}S_{80}X_{48}$ CQDs, where X is X-type ligand with increasing electronegativities: methanethiol (2.45), I (2.66), Br (2.96), and Cl (3.16). The effective electronegativities of X are in Pauling units χ. (b) The FC shifts and average atom displacements of various defects, with s (surface), c (core), e (edge) indicating their locations on the CQDs.

of the CQDs (Figures S1−3). Therefore, the core atoms, defined as atoms with six nearest neighbors, exhibited higher displacements than the surface atoms. The atomic displacements are higher with ligands with larger electronegativities. In particular, most of the ligands passivate the {111} facet, which makes almost no contribution to the CBM and VBM states; hence, the FC shifts are resistant to ligand changes.

The inclusion of spin−orbit coupling (SOC) effects are important for heavy elements such as Pb.[48] However, while the inclusion of SOC effects lowered the FC shifts by about 10 meV, the trends are well described without SOC (Table S1). In addition, we examined cases of other CQD geometries and ligand types by performing calculations using a series of cubic CQDs with L-type ligands. The results are summarized in Supporting Information and in general show similar trends as for the cases discussed above (Figure S4).

Defects. One key advantage of PbS CQDs over existing PV technologies is their low-cost and scalable solution-based synthesis.[32,38,49] However, during the synthesis process, many structural defects and surface impurities inevitably form, some of which can cause detrimental impacts on the electronic and optical properties.[42,50] As these defects may cause large electron density localizations, we here systematically investigated their effects on the FC shifts. Three types of defects, that is, (1) small molecular species adsorbed onto the CQD surfaces, (2) Schottky defects where a neutral stoichiometric vacancy pair is removed, and (3) elementary vacancies, were studied. All defects were created from the Cl-passivated CQD $Pb_{104}S_{80}Cl_{48}$ and produced no midgap states (Figure 4a).

For the first type of defect, we placed water molecules (H_2O) on the {100} facet of the CQDs. The FC shifts are similar to the defect-free nanocrystal at approximately 60 meV (Figure 3b). Next, we created stoichiometric Schottky pairs by removing either PbS or $PbCl_2$ atoms from the CQD surfaces. The FC shifts from these defects are also small and comparable to the defect-free nanocrystal. For both surface water molecules and surface vacancies V_{PbS} and V_{PbCl_2}, varying the locations of the defects had negligible impacts on the FC shifts. In both cases, modifying the CQD surfaces has little impact on the overall electron densities of the CBM and VBM states, which are delocalized in the CQD core. Notably, the FC shift from V_{PbS} is approximately 10 meV higher than that of V_{PbCl_2}. This is because PbS atoms were removed from the {100} facet, which
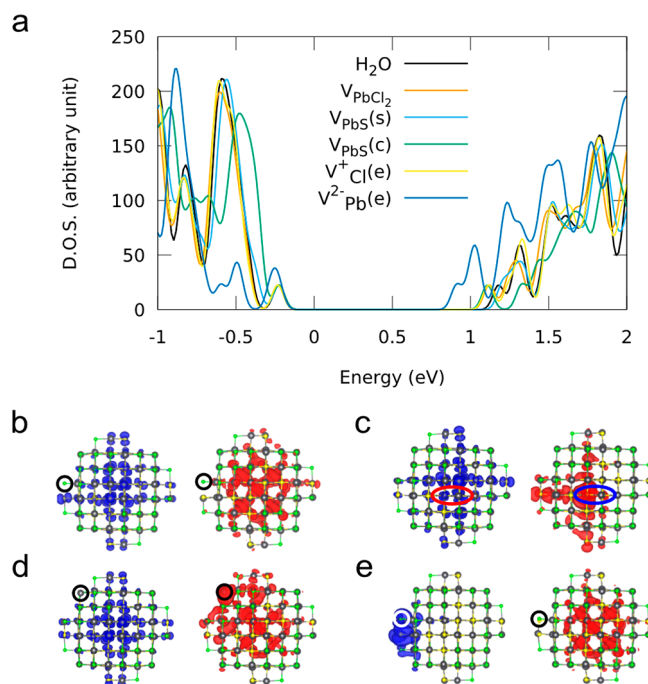
Figure 4. (a) Density of states for defects in Cl-passivated PbS CQDs for various defects, all of which exhibit no midgap trap states. Charge density distribution for the CBM and VBM for (b) V_{PbS} (s), (c) V_{PbS} (c), (d) V_{Cl}^+ and (e) V_{Pb}^{2-}; s (surface), c (core), and e (edge) indicate the locations of the defects, which are also highlighted with circles.

has a larger electron density than the {111} facet from which the $PbCl_2$ atoms were removed.

When a PbS Schottky pair is created by removing atoms from the nanocrystal core, the resulting FC shift is significantly higher at 524 meV. Removing core atoms led to a large localization of the electron densities of the CBM, which resulted in the exertion of large excited-state forces on the core atoms (Figure 4c). However, it is prohibitively expensive to create a PbS vacancy pair at the interior of the CQD, as its formation energy is approximately 0.90 eV higher than its counterpart on the surface. We do not expect core vacancies to be present in PbS CQDs, as a strong driving force would move the defect from the core to the surface.[42]

Finally, we investigated various charged elementary defects. In the presence of a counterion in the reaction solution, the formation of charged defects is much more favorable than the formation of their neutral counterparts.[42] As the ionic vacancies are created, the nanocrystal will be bound to counteranions in the solution. Among the defects, V_{Pb}^{2-} and V_{Cl}^{+} do not produce midgap states, whereas V_{S}^{2+} does. In our study, we will focus on V_{Cl}^{+} and V_{Pb}^{2-}, as having a trap-free band gap improves the convergence behavior of the triplet state under constrained DFT calculation.

Three structures with V_{Cl}^{+} and V_{Pb}^{2-} vacancies were created by removing Cl^{-} and Pb^{2+} ions from the corner, edge, and center of the {111} and {100} facets, respectively. Their relative formation energies and resulting FC shifts are summarized in Table 1. For V_{Pb}^{2-}, we see that both the stable V_{Pb}^{2-} (center) and

Table 1. Relative Formation Energies and FC Shifts of the Three V_{Pb}^{2-} and V_{Cl}^{+} Defects at Different Locations on the {100} and {111} Facets of the $Pb_{104}S_{80}Cl_{48}$ CQD

defects	relative formation energy (meV)	FC shift (meV)
defect free	NA	66
V_{Pb}^{2-} (center)	0	66
V_{Pb}^{2-} (corner)	80	64
V_{Pb}^{2-} (edge)	1250	843
V_{Cl}^{+} (corner)	0	66
V_{Cl}^{+} (edge)	52	718
V_{Cl}^{+} (center)	114	811

V_{Pb}^{2-} (corner) exhibited small FC shifts. Although V_{Pb}^{2-} (edge) exhibited FC shifts >840 meV, its relative formation energy is prohibitively large. In contrast, V_{Cl}^{+} (corner) and V_{Cl}^{+} (middle) exhibited large FC shifts of over 700 and 800 meV, respectively, with formation energies only 52 and 114 meV higher than the most stable defect structure. At the synthesis temperature of 150 °C, a simple Arrhenius relation $k \sim e^{-\Delta E/kT}$ gives formation rates of V_{Cl}^{+} (corner) to V_{Cl}^{+} (edge) and V_{Cl}^{+} (center) of approximately 25:5:1.

To understand why certain V_{Pb}^{2-} and V_{Cl}^{+} cause large FC shifts, we visualized their electron densities. The CBM mainly consists of Pb(6p) orbital contributions, and the breaking of the Pb−Cl bond when removing the surface Cl atom results in charge localization around the defect site (Figure 4d). For V_{Pb}^{2-} (edge), the breaking of the Pb−S bond as a result of Pb atom removal significantly localizes the electron density around the sulfur atoms due to its S(3p) character (Figure 4e). For both defects, the mean atomic displacements of the surface atoms are larger than those of core atoms because of the increased excited-state forces around the surface defects (Figure 3b). In addition, we calculated the FC shifts of the three V_{Cl}^{+} with the inclusion of SOC effects (Table S1). While the overall shifts are lowered by 150 to 200 meV compared to non-SOC results, this does not change our observation that defects cause a substantial increase in FC shifts on the order of hundreds of meV.

The Stokes shift of PbS CQDs is size-dependent in the quantum confined regime: It decreases as the CQD size increase.[20,47] It has been reported that the Stokes shifts of PbS CQDs at 1−2 nm can be as large as 580 meV.[51] At this size, the combined contribution from dark exciton effects and FC shifts are only approximately 100 meV. Our calculations with intrinsic defects (V_{Cl}^{+}) lead to substantial amounts of FC shift, which can reconcile the experimentally measured and theoretical Stokes shift. Our work also agrees with recent work on CdSe CQDs

that showed that strong vibronic contributions from surface states are important at controlling the Stokes shift in CQDs.[11]

While our experimental and computational results cannot be compared directly due to the different CQD sizes, we can speculate that the increased defect densities from ligand exchange processes might be responsible for higher Stokes shifts. This result in turn suggests that by elimination of the defects and electron localization, the Stokes shift can be lowered to enhance PbS CQD-based device performance. In addition to defects, the morphology and surface structures of CQDs might change significantly during CQDs synthesis and ligand exchanges process,[52] which might warrant further investigation in the future.

CONCLUSION

In summary, we have used a combination of UV−vis and PL spectroscopy with *ab initio* calculations to investigate the Stokes shift of PbS CQD in order to understand the origins of the excessive Stokes shift in PbS nanocrystals. We found that the size and energetic disorders in a polydisperse CQD solid film contribute to an increase in the Stokes shift of approximately 20 to 50 meV compared to isolated CQDs. As we change the surface passivation, higher FC shifts are observed for ligands with larger electronegativities, but this effect is very small. Some stable intrinsic defects, such as V_{Cl}^{+}, can cause large electron localizations in the CBM states and excessive FC shifts comparable to experimental values. This increased shift is sufficient to explain the excessive Stokes shift. Our results indicate that the FC shift is likely to be an important source of the large Stokes shift in the lead chalcogenide family of CQDs, and this improved understanding of the optical properties of PbS CQDs is of great importance when designing the next generation of PV applications.

METHODS

DFT Calculation. All DFT calculations were performed using the Vienna Ab Initio Simulation Package.[53,54] Electronic wave functions were expanded in plane-wave basis sets with an energy cutoff of 400 eV. We applied the Perdew−Burke−Ernzerhof-type generalized gradient approximation to the exchange−correlation functional,[55] and the core−valence interaction was treated using the projected augmented wave method.[56] A vacuum spacing of 15 Å was added to the supercell in all 3 spatial directions to remove any spurious interactions. Only the Γ k-point in the Brillouin zone was sampled, and the atomic positions were relaxed until the residual forces were <0.01 eV/Å. Electronic wave functions were visualized using the VESTA program.[57]

We follow the same approach as in previous work for the calculation of the FC shift.[5,6] The ground-state atomic configuration and total energy $E^{gs}(\mathbf{R}_{gs})$ is first obtained by minimizing the quantum mechanical forces. An electron−hole pair is excited in the triplet state, and the excited-state energy in the ground-state geometry is obtained $E^{t}(\mathbf{R}_{gs})$. The atomic positions are relaxed in the triplet spin configuration using constrained DFT, which gives the excited-state total energy in the excited-state geometry $E^{t}(\mathbf{R}_{xs})$. Finally, we calculate the ground-state total energy in the excited-state geometry $E^{gs}(\mathbf{R}_{xs})$. We note that after the vertical excitation from $E^{gs}(\mathbf{R}_{xs})$, the correct spin state is the singlet state with energy $E^{s}(\mathbf{R}_{xs})$; however, the energy difference between the bright spin-singlet and dark spin-triplet states has been demonstrated to be typically only 17 and 2 meV for PbSe CQDs[21] with diameters of 1.5 and 3 nm, respectively. Adopting the triplet spin configuration greatly improves the convergence behavior of our calculations.[5]

The FC shift is given by

$$\Delta E_{fc} = [E^{t}(\mathbf{R}_{gs}) - E^{gs}(\mathbf{R}_{gs})] - [E^{t}(\mathbf{R}_{xs}) - E^{gs}(\mathbf{R}_{xs})]$$

CQD Synthesis and Ligand Exchange. PbS CQDs were synthesized according to a modified procedure from the literature.[58] Ligand exchanges were achieved by adapting various two-phase solution exchange methods.[59−61] Iodine-capped CQDs were prepared by combining 1 mL of CQDs (10 mg/mL in octane) with 0.75 mL of NaI (150 mg/mL in MeCN). The phases were mixed by vigorous shaking for at least 5 min and then left to stand until the CQDs had separated into the bottom MeCN layer. 3-Mercaptopropionic acid (MPA)-capped CQDs were prepared by combining 0.5 mL of CQDs (2.5 mg/mL in octane) with 0.5 mL of MPA (60 mg/mL in DMSO). The phases were vortexed at high speed for 2 min and then left to stand, whereupon the CQDs separated into the bottom DMSO layer. 1-Thioglycerol (TG)-capped CQDs were prepared by combining 0.5 mL of CQDs (4 mg/mL in octane) with 0.5 mL of TG (21 mg/mL in DMSO). The phases were vortexed at high speed for 5 s, visually initiating the exchange, and then were immediately centrifuged at 3200 rpm for 2 min. When removed from the centrifuge, the CQDs had migrated to the bottom DMSO solution. All three exchanged solutions were washed to remove residual oleic acid (OA) by repeating the relevant mixing step with the top octane layers.

Stokes Shift Measurements. CQD films were fabricated by diluting each CQD solution to 2.5 mg/mL and then drop casting them onto quartz disks through a 0.2 μm filter. For solution phase measurements, each solution was diluted to 1 mg/mL and then transferred into a quartz cuvette. Absorption measurements were performed using a Cary 5000 UV−vis−NIR spectrophotometer, whereas PL measurements were performed using a ThorLabs DET10N InGaAs detector and a 5 mW 532 nm excitation laser.

ASSOCIATED CONTENT

⑤ Supporting Information

The Supporting Information is available free of charge on the ACS Publications website at DOI: 10.1021/acsnano.8b00132.

> Figures showing the electronic structures of defects-free CQDs passivated with Br, I, and methanethiol ligands. Table and discussions showing the impacts of including SOC effects on the FC shifts of CQDs with and without defects. Schemes and figures showing the design of the L-type ligands and their impacts on the FC shifts of cubic CQDs (PDF)

AUTHOR INFORMATION

Corresponding Author

*E-mail: jcg@mit.edu.

ORCID ⑩

Yun Liu: 0000-0003-1630-4052

Donghun Kim: 0000-0003-0326-5381

Author Contributions

§These authors contributed equally.

Notes

The authors declare no competing financial interest.

ACKNOWLEDGMENTS

REFERENCES

(1) Meinardi, F.; Colombo, A.; Velizhanin, K. A.; Simonutti, R.; Lorenzon, M.; Beverina, L.; Viswanatha, R.; Klimov, V. I.; Brovelli, S. Large-Area Luminescent Solar Concentrators Based on "Stokes-Shift-Engineered" Nanocrystals in a Mass-Polymerized PMMA Matrix. *Nat. Photonics* **2014**, *8*, 392−399.

(2) Li, C.; Chen, W.; Wu, D.; Quan, D.; Zhou, Z.; Hao, J.; Qin, J.; Li, Y.; He, Z.; Wang, K. Large Stokes Shift and High Efficiency Luminescent Solar Concentrator Incorporated with CuInS2/ZnS Quantum Dots. *Sci. Rep.* **2016**, *5*, 17777.

(3) Ushakova, E. V.; Litvin, A. P.; Parfenov, P. S.; Fedorov, A. V.; Artemyev, M.; Prudnikau, A. V.; Rukhlenko, I. D.; Baranov, A. V. Anomalous Size-Dependent Decay of Low-Energy Luminescence from PbS Quantum Dots in Colloidal Solution. *ACS Nano* **2012**, *6*, 8913−8921.

(4) Bagga, A.; Chattopadhyay, P. K.; Ghosh, S. Origin of Stokes Shift in InAs and CdSe Quantum Dots: Exchange Splitting of Excitonic States. *Phys. Rev. B: Condens. Matter Mater. Phys.* **2006**, *74*, 35341.

(5) Puzder, A.; Williamson, A. J.; Grossman, J. C.; Galli, G. Computational Studies of the Optical Emission of Silicon Nanocrystals. *J. Am. Chem. Soc.* **2003**, *125*, 2786−2791.

(6) Franceschetti, A.; Pantelides, S. T. Excited-State Relaxations and Franck-Condon Shift in Si Quantum Dots. *Phys. Rev. B: Condens. Matter Mater. Phys.* **2003**, *68*, 33313.

(7) Korkusinski, M.; Voznyy, O.; Hawrylak, P. Fine Structure and Size Dependence of Exciton and Biexciton Optical Spectra in CdSe Nanocrystals. *Phys. Rev. B: Condens. Matter Mater. Phys.* **2010**, *82*, 245304.

(8) Nirmal, M.; Norris, D. J.; Kuno, M.; Bawendi, M. G.; Efros, A. L.; Rosen, M. Observation of the "Dark Exciton" in CdSe Quantum Dots. *Phys. Rev. Lett.* **1995**, *75*, 3728−3731.

(9) Norris, D. J.; Efros, A.; Rosen, M.; Bawendi, M. Size Dependence of Exciton Fine Structure in CdSe Quantum Dots. *Phys. Rev. B: Condens. Matter Mater. Phys.* **1996**, *53*, 16347−16354.

(10) Efros, A. L.; Rosen, M.; Kuno, M.; Nirmal, M.; Norris, D.; Bawendi, M. Band-Edge Exciton in Quantum Dots of Semiconductors with a Degenerate Valence Band: Dark and Bright Exciton States. *Phys. Rev. B: Condens. Matter Mater. Phys.* **1996**, *54*, 4843−4856.

(11) Mack, T. G.; Jethi, L.; Kambhampati, P. Temperature Dependence of Emission Line Widths from Semiconductor Nanocrystals Reveals Vibronic Contributions to Line Broadening Processes. *J. Phys. Chem. C* **2017**, *121*, 28537−28545.

(12) Mooney, J.; Krause, M. M.; Saari, J. I.; Kambhampati, P. A Microscopic Picture of Surface Charge Trapping in Semiconductor Nanocrystals. *J. Chem. Phys.* **2013**, *138*, 204705.

(13) Jethi, L.; Mack, T. G.; Kambhampati, P. Extending Semiconductor Nanocrystals from the Quantum Dot Regime to the Molecular Cluster Regime. *J. Phys. Chem. C* **2017**, *121*, 26102−26107.

(14) Jethi, L.; Mack, T. G.; Krause, M. M.; Drake, S.; Kambhampati, P. The Effect of Exciton-Delocalizing Thiols on Intrinsic Dual Emitting Semiconductor Nanocrystals. *ChemPhysChem* **2016**, *17*, 665−669.

(15) Sagar, D. M.; Cooney, R. R.; Sewall, S. L.; Dias, E. A.; Barsan, M. M.; Butler, I. S.; Kambhampati, P. Size Dependent, State-Resolved Studies of Exciton-Phonon Couplings in Strongly Confined Semiconductor Quantum Dots. *Phys. Rev. B: Condens. Matter Mater. Phys.* **2008**, *77*, 235321.

(16) Mooney, J.; Saari, J. I.; Myers Kelley, A.; Krause, M. M.; Walsh, B. R.; Kambhampati, P. Control of Phonons in Semiconductor Nanocrystals *via* Femtosecond Pulse Chirp-Influenced Wavepacket Dynamics and Polarization. *J. Phys. Chem. B* **2013**, *117*, 15651−15658.

(17) Fernée, M. J.; Thomsen, E.; Jensen, P.; Rubinsztein-Dunlop, H. Highly Efficient Luminescence from a Hybrid State Found in Strongly Quantum Confined PbS Nanocrystals. *Nanotechnology* **2006**, *17*, 956−962.

(18) Schaller, R. D.; Crooker, S. A.; Bussian, D. A.; Pietryga, J. M.; Joo, J.; Klimov, V. I. Revealing the Exciton Fine Structure of PbSe Nanocrystal Quantum Dots Using Optical Spectroscopy in High Magnetic Fields. *Phys. Rev. Lett.* **2010**, *105*, 67403.

(19) Leitsmann, R.; Bechstedt, F. Characteristic Energies and Shifts in Optical Spectra of Colloidal IV-VI Semiconductor Nanocrystals. *ACS Nano* **2009**, *3*, 3505–3512.

(20) Grinolds, D. D. W.; Brown, P. R.; Harris, D. K.; Bulovic, V.; Bawendi, M. G. Quantum-Dot Size and Thin-Film Dielectric Constant: Precision Measurement and Disparity with Simple Models. *Nano Lett.* **2015**, *15*, 21–26.

(21) An, J. M.; Franceschetti, A.; Dudiy, S. V.; Zunger, A. The Peculiar Electronic Structure of PbSe Quantum Dots. *Nano Lett.* **2006**, *6*, 2728–2735.

(22) An, J. M.; Franceschetti, A.; Zunger, A. The Excitonic Exchange Splitting and Radiative Lifetime in PbSe Quantum Dots. *Nano Lett.* **2007**, *7* (7), 2129–2135.

(23) Caram, J. R.; Bertram, S. N.; Utzat, H.; Hess, W. R.; Carr, J. A.; Bischof, T. S.; Beyler, A. P.; Wilson, M. W. B.; Bawendi, M. G. PbS Nanocrystal Emission Is Governed by Multiple Emissive States. *Nano Lett.* **2016**, *16*, 6070–6077.

(24) Voznyy, O.; Levina, L.; Fan, F.; Walters, G.; Fan, J. Z.; Kiani, A.; Ip, A. H.; Thon, S. M.; Proppe, A. H.; Liu, M.; Sargent, E. H. Origins of Stokes Shift in PbS Nanocrystals. *Nano Lett.* **2017**, *17*, 7191–7195.

(25) Zhitomirsky, D.; Voznyy, O.; Hoogland, S.; Sargent, E. H. Measuring Charge Carrier Diffusion in Coupled Colloidal Quantum Dot Solids. *ACS Nano* **2013**, *7*, 5282–5290.

(26) Lee, S.; Zhitomirsky, D.; Grossman, J. C. Manipulating Electronic Energy Disorder in Colloidal Quantum Dot Solids for Enhanced Charge Carrier Transport. *Adv. Funct. Mater.* **2016**, *26*, 1554–1562.

(27) Zhitomirsky, D.; Kramer, I. J.; Labelle, A. J.; Fischer, A.; Debnath, R.; Pan, J.; Bakr, O. M.; Sargent, E. H. Colloidal Quantum Dot Photovoltaics: The Effect of Polydispersity. *Nano Lett.* **2012**, *12* (2), 1007–1012.

(28) Murray, C. B.; Kagan, C. R.; Bawendi, M. G. Synthesis and Characterization of Monodisperse Nanocrystals and Close-Packed Nanocrystal Assemblies. *Annu. Rev. Mater. Sci.* **2000**, *30*, 545–610.

(29) Weidman, M. C.; Beck, M. E.; Hoffman, R. S.; Prins, F.; Tisdale, W. A. Monodisperse, Air-Stable PbS Nanocrystals *via* Precursor Stoichiometry Control. *ACS Nano* **2014**, *8*, 6363–6371.

(30) Gilmore, R. H.; Lee, E. M. Y.; Weidman, M. C.; Willard, A. P.; Tisdale, W. A. Charge Carrier Hopping Dynamics in Homogeneously Broadened PbS Quantum Dot Solids. *Nano Lett.* **2017**, *17* (2), 893–901.

(31) Kim, J. Y.; Voznyy, O.; Zhitomirsky, D.; Sargent, E. H. 25th Anniversary Article: Colloidal Quantum Dot Materials and Devices: A Quarter-Century of Advances. *Adv. Mater.* **2013**, *25*, 4986–5010.

(32) Carey, G. H.; Abdelhady, A. L.; Ning, Z.; Thon, S. M.; Bakr, O. M.; Sargent, E. H. Colloidal Quantum Dot Solar Cells. *Chem. Rev.* **2015**, *115*, 12732–12763.

(33) Brown, P. R.; Kim, D.; Lunt, R. R.; Zhao, N.; Bawendi, M. G.; Grossman, J. C.; Bulovi, V. Energy Level Modification in Lead Sulfide Quantum Dot Thin Films through Ligand Exchange. *ACS Nano* **2014**, *8*, 5863–5872.

(34) Chuang, C.-H. M.; Brown, P. R.; Bulović, V.; Bawendi, M. G. Improved Performance and Stability in Quantum Dot Solar Cells through Band Alignment Engineering. *Nat. Mater.* **2014**, *13*, 796–801.

(35) Manna, L.; Scher, E. C.; Alivisatos, A. P. Synthesis of Soluble and Processable Rod-, Arrow-, Teardrop-, and Tetrapod-Shaped CdSe Nanocrystals. *J. Am. Chem. Soc.* **2000**, *122*, 12700–12706.

(36) Giansante, C.; Infante, I.; Fabiano, E.; Grisorio, R.; Suranna, G. P.; Gigli, G. Darker-than-Black" PbS Quantum Dots: Enhancing Optical Absorption of Colloidal Semiconductor Nanocrystals *via* Short Conjugated Ligands. *J. Am. Chem. Soc.* **2015**, *137*, 1875–1886.

(37) Anderson, N. C.; Hendricks, M. P.; Choi, J. J.; Owen, J. S. Ligand Exchange and the Stoichiometry of Metal Chalcogenide Nanocrystals: Spectroscopic Observation of Facile Metal-Carboxylate

Displacement and Binding. *J. Am. Chem. Soc.* **2013**, *135*, 18536–18548.

(38) Tang, J.; Brzozowski, L.; Barkhouse, D. A. R.; Wang, X.; Debnath, R.; Wolowiec, R.; Palmiano, E.; Levina, L.; Pattantyus-Abraham, A. G.; Jamakosmanovic, D.; Sargent, E. H. Quantum Dot Photovoltaics in the Extreme Quantum Confinement Regime: The Surface-Chemical Origins of Exceptional Air- and Light-Stability. *ACS Nano* **2010**, *4*, 869–878.

(39) Lan, X.; Voznyy, O.; García De Arquer, F. P.; Liu, M.; Xu, J.; Proppe, A. H.; Walters, G.; Fan, F.; Tan, H.; Liu, M.; Yang, Z.; Hoogland, S.; Sargent, E. H. 10.6% Certified Colloidal Quantum Dot Solar Cells *via* Solvent-Polarity-Engineered Halide Passivation. *Nano Lett.* **2016**, *16*, 4630–4634.

(40) Moreels, I.; Lambert, K.; De Muynck, D.; Vanhaecke, F.; Poelman, D.; Martins, J. C.; Allan, G.; Hens, Z. Composition and Size-Dependent Extinction Coefficient of Colloidal PbSe Quantum Dots Composition and Size-Dependent Extinction Coefficient of Colloidal PbSe Quantum Dots. *Chem. Mater.* **2007**, *19*, 6101–6106.

(41) Zherebetskyy, D.; Scheele, M.; Zhang, Y.; Bronstein, N.; Thompson, C.; Britt, D.; Salmeron, M.; Alivisatos, P.; Wang, L.-W. Hydroxylation of the Surface of PbS Nanocrystals Passivated with Oleic Acid. *Science (Washington, DC, U. S.)* **2014**, *344* (80), 1380–1384.

(42) Zherebetskyy, D.; Zhang, Y.; Salmeron, M.; Wang, L.-W. Tolerance of Intrinsic Defects in PbS Quantum Dots. *J. Phys. Chem. Lett.* **2015**, *6*, 4711–4716.

(43) Choi, H.; Ko, J.; Kim, Y.; Jeong, S. Steric Hindrance Driven Shape Transition in PbS Quantum Dots: Understanding Size-Dependent Stability. *J. Am. Chem. Soc.* **2013**, *135*, 5278–5281.

(44) Kim, D.; Kim, D. H.; Lee, J. H.; Grossman, J. C. Impact of Stoichiometry on the Electronic Structure of PbS Quantum Dots. *Phys. Rev. Lett.* **2013**, *110*, 196802.

(45) Carey, G. H.; Kramer, I. J.; Kanjanaboos, P.; Moreno-Bautista, G.; Voznyy, O.; Rollny, L.; Tang, J. A.; Hoogland, S.; Sargent, E. H. Electronically Active Impurities in Colloidal Quantum Dot Solids. *ACS Nano* **2014**, *8*, 11763–11769.

(46) Somayajulu, G. R. Dependence of Force Constant on Electronegativity, Bond Strength, and Bond Order. VII. *J. Chem. Phys.* **1958**, *28*, 814.

(47) Litvin, A. P.; Parfenov, P. S.; Ushakova, E. V.; Fedorov, A. V.; Artemyev, M. V.; Prudnikau, A. V.; Golubkov, V. V.; Baranov, A. V. PbS Quantum Dots in a Porous Matrix: Optical Characterization. *J. Phys. Chem. C* **2013**, *117*, 12318–12324.

(48) Wei, S. H.; Zunger, A. Electronic and Structural Anomalies in Lead Chalcogenides. *Phys. Rev. B: Condens. Matter Mater. Phys.* **1997**, *55*, 13605–13610.

(49) Cao, Y.; Stavrinadis, A.; Lasanta, T.; So, D.; Konstantatos, G. The Role of Surface Passivation for Efficient and Photostable PbS Quantum Dot Solar Cells. *Nat. Energy* **2016**, *1*, 16035.

(50) Zhang, Y.; Zherebetskyy, D.; Bronstein, N. D.; Barja, S.; Lichtenstein, L.; Alivisatos, A. P.; Wang, L.-W.; Salmeron, M. Molecular Oxygen Induced in-Gap States in PbS Quantum Dots. *ACS Nano* **2015**, *9*, 10445–10452.

(51) Warner, J. H.; Thomsen, E.; Watt, A. R.; Heckenberg, N. R.; Rubinsztein-Dunlop, H. Time-Resolved Photoluminescence Spectroscopy of Ligand-Capped PbS Nanocrystals. *Nanotechnology* **2005**, *16*, 175–179.

(52) Peters, J. L.; Van Den Bos, K. H. W.; Van Aert, S.; Goris, B.; Bals, S.; Vanmaekelbergh, D. Ligand-Induced Shape Transformation of PbSe Nanocrystals. *Chem. Mater.* **2017**, *29*, 4122–4128.

(53) Kresse, G.; Furthmüller, J. Efficient Iterative Schemes for *Ab Initio* Total-Energy Calculations Using a Plane-Wave Basis Set. *Phys. Rev. B: Condens. Matter Mater. Phys.* **1996**, *54*, 11169–11186.

(54) Kresse, G.; Furthmüller, J. Efficiency of Ab-Initio Total Energy Calculations for Metals and Semiconductors Using a Plane-Wave Basis Set. *Comput. Mater. Sci.* **1996**, *6*, 15–50.

(55) Perdew, J. P.; Burke, K.; Ernzerhof, M. Generalized Gradient Approximation Made Simple. *Phys. Rev. Lett.* **1996**, *77*, 3865–3868.

(56) Kresse, G.; Joubert, D. From Ultrasoft Pseudopotentials to the Projector Augmented-Wave Method. *Phys. Rev. B: Condens. Matter Mater. Phys.* **1999**, *59*, 1758−1775.

(57) Momma, K.; Izumi, F. VESTA: A Three-Dimensional Visualization System for Electronic and Structural Analysis. *J. Appl. Crystallogr.* **2008**, *41*, 653−658.

(58) Hines, M. A.; Scholes, G. D. Colloidal PbS Nanocrystals with Size-Tunable Near-Infrared Emission: Observation of Post-Synthesis Self-Narrowing of the Particle Size Distribution. *Adv. Mater.* **2003**, *15*, 1844−1849.

(59) Ning, Z.; Dong, H.; Zhang, Q.; Voznyy, O.; Sargent, E. H. Solar Cells Based on Inks of N-Type Colloidal Quantum Dots. *ACS Nano* **2014**, *8*, 10321−10327.

(60) Kim, J. Y.; Adinolfi, V.; Sutherland, B. R.; Voznyy, O.; Kwon, S. J.; Kim, T. W.; Kim, J.; Ihee, H.; Kemp, K.; Adachi, M.; Yuan, M.; Kramer, I.; Zhitomirsky, D.; Hoogland, S.; Sargent, E. H. Single-Step Fabrication of Quantum Funnels *via* Centrifugal Colloidal Casting of Nanoparticle Films. *Nat. Commun.* **2015**, *6*, 7772.

(61) Fischer, A.; Rollny, L.; Pan, J.; Carey, G. H.; Thon, S. M.; Hoogland, S.; Voznyy, O.; Zhitomirsky, D.; Kim, J. Y.; Bakr, O. M.; Sargent, E. H. Directly Deposited Quantum Dot Solids Using a Colloidally Stable Nanoparticle Ink. *Adv. Mater.* **2013**, *25*, 5742−5749.

H